Available online at www.sciencedirect.com

SciVerse ScienceDirect

journal homepage: www.elsevier.com/locate/he

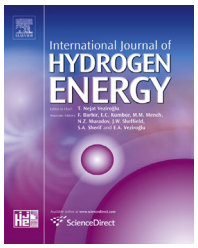

Effect of multi-bend geometry on deflagration to detonation transition of a hydrocarbon-air mixture in tubes

*Min-cheol Gwak, Jack J. Yoh**

School of Mechanical and Aerospace Engineering, Seoul National University, 1 Gwanakro, Gwanakgu, Seoul 151-742, Republic of Korea

ARTICLE INFO

Article history:
Received 15 May 2013
Received in revised form
19 June 2013
Accepted 24 June 2013
Available online 17 July 2013

Keywords:
Deflagration-to-detonation transition
Hydrocarbon mixture
Multi-bend tube
Safety hazard

ABSTRACT

We present a numerical investigation of gaseous deflagration-to-detonation transition (DDT) triggered by a shock in a multi-bend geometry. The ethylene-air mixture filled rigid tube with obstacles is considered for understanding the effects of complex confinement and initial flame size on DDT. Our calculations show generation of hot spots by flame and strong shock interactions, and flame propagation is either restrained or accelerated due to the wall obstacles of both straight and bent tubes. The effect of initial flame size on DDT in complex confinement geometry is analyzed as well as the hot spot formation on promoting shock–flame interaction, leading to a full detonation.

1. Introduction

The combustion phenomenon addressed in the present study concerns two modes of burning: deflagration and detonation. The detonation results in a rapid increase of pressure, temperature, and propagation speed of flame, leading to an extreme thermodynamic state within a very short time. When accompanied by structural failure, accidental detonation transition is a significant safety concern. Also, detonation in a fuel pipe can cause rupture or fracture that can lead to catastrophic disaster [1,2]. For this reason, deflagration-to-detonation transition (DDT) has maintained continued interest in the combustion community for experimental, theoretical, and numerical investigations [3–6].

DDT is an extremely complicated process involving deflagrations, shocks, reflected shocks, boundary layers, and their interactions. In the literature, there are known mechanisms of DDT as addressed in recent years. The Richtmyer-Meshkov (RM) instability resulting from repeated shock–flame interactions and bifurcated structure formed by reflected shock and boundary layer interaction generates turbulent flames. The turbulent flames create conditions in a nearby unreacted gas, which leads to generation of hot spots for developing a detonation through the Zel'dovich gradient mechanism [7].

* *Corresponding author*. Tel.: +82 2 880 9334.
E-mail address: jjyoh@snu.ac.kr (J.J. Yoh).

0360-3199
http://dx.doi.org/10.1016/j.ijhydene.2013.06.108

The temperature gradient triggers DDT at localized hot spots that are formed ahead of the flame front. Both modes of burning can be expressed by a single-step chemical reaction which satisfies the characteristic length and time of deflagration and detonation [4]. Another view on the DDT mechanism suggests that a temperature gradient mechanism is unnecessary, and that a multi-step chemical reaction must be considered. The pressure amplified by the positive feedback between the pressure rise and the enhanced reaction in the front edge of the flame would lead to preheat zone formation and flame acceleration, responsible for such transition to detonation [6].

These rather distinct views on the mechanism have something in common: the interaction between a strong shock wave, and the critical role of flame acceleration leading to DDT. In most laboratory experiments, the onset of DDT is believed to originate somewhere within the strange shock structure enhanced by the multiple interactions of the shock, reflected shock, and flame. This shock–flame interaction can be strengthened when encountered by complex geometries such as walls, obstacles, and curves within pipes due to multiple reflections of shocks and expanded flame surfaces.

In view of the shock–flame interaction being the main cause of DDT, researchers have looked at such phenomena in pipes in order to gain better understanding of geometrical factors responsible for DDT. In Refs. [4] and [5], comprehensive reviews on the gaseous DDT induced from the shock–flame interaction in straight tube are discussed. A consideration of the effect of obstacles is made in Refs. [5], where the enhancement of shock–flame interactions, instabilities, and flame–vortex interaction in obstacle wakes brings about the growth of the flame surface, the energy-release rate, and the intensity of the shock. Also the change in DDT triggering time and position due to the obstacle spacing and size was shown. With an emphasis on the effect of curves within pipes [8], and [9] showed how the curvature and tube diameter in a U-bend tube change the detonation propagation characteristics. Although these studies showed valuable information on a fully developed detonation in tubes, the transition study from a deflagration to a detonation subject to complex confinement geometries has not been addressed until now.

We investigate DDT in a multi-bend geometry with obstacles for comparison to a straight geometry to understand the factors responsible for triggering flame acceleration and termination. Since the initial flame size is indicative of flame surface condition [4], different flame size in two-dimensional tube geometry is also considered to provide insight into the transition dynamics of gaseous deflagrations.

2. Numerical model

2.1. Formulation of the problem

To simulate the DDT process, we solved multidimensional, time-dependent, and reactive compressible Navier–Stokes equations, which include models for viscosity, thermal conduction, molecular diffusion, and chemical reaction. Equations (1)–(6) are the conservation equations of mass, x-axis momentum, y-axis momentum, energy, and species, and the equation of state of ideal gas in a two-dimensional rectangular coordinate:

$$\frac{\partial \rho}{\partial t}+\frac{\partial}{\partial x}(\rho u)+\frac{\partial}{\partial y}(\rho v)=0 \tag{1}$$

$$\frac{\partial}{\partial t}(\rho u)+\frac{\partial}{\partial x}\left(\rho u^2+P\right)+\frac{\partial}{\partial x}(\rho uv)=\frac{\partial \tau_{xx}}{\partial x}+\frac{\partial \tau_{yx}}{\partial y} \tag{2}$$

$$\frac{\partial}{\partial t}(\rho v)+\frac{\partial}{\partial x}(\rho uv)+\frac{\partial}{\partial y}\left(\rho v^2+P\right)=\frac{\partial \tau_{xy}}{\partial x}+\frac{\partial \tau_{yy}}{\partial y} \tag{3}$$

$$\begin{aligned}\frac{\partial}{\partial t}(\rho e)+\frac{\partial}{\partial x}[u(\rho e+P)]+\frac{\partial}{\partial y}[v(\rho e+P)]&=\frac{\partial\left(u\tau_{xx}+u_y\tau_{xy}-q_x\right)}{\partial x}\\&+\frac{\partial\left(u_x\tau_{yx}+u_y\tau_{yy}-q_y\right)}{\partial y}+\rho Q_i\dot{w}_i\end{aligned} \tag{4}$$

$$\frac{\partial}{\partial t}(\rho Y_i)+\frac{\partial}{\partial x}(\rho Y_i u)+\frac{\partial}{\partial y}(\rho Y_i v)=-\frac{\partial d_x}{\partial x}-\frac{\partial d_y}{\partial y}+\rho\dot{w}_i \tag{5}$$

$$P=\frac{\rho RT}{M} \tag{6}$$

where ρ, u, v, P, e, Y_i, R, and M are density, x-axis velocity, y-axis velocity, pressure, total energy density, mass fraction of a reactant, the universal gas constant, and molecular weight, respectively. In the source term, $\vec{q}=k\nabla T$ is the thermal conduction, $\dot{w}_i\equiv\partial Y_i/\partial t|_{Chem}=A\rho Y\exp(-E_a/(RT))$ is the reaction rate described by the first-order Arrhenius kinetics, $\vec{d}=\rho D\nabla Y_i$ is the mass diffusion, and τ_{xx}, $\tau_{xy}=\tau_{yx}$, and τ_{yy} are the viscous stresses that are calculated by constitutive relation. Here, k is the thermal conduction coefficient, A is the pre-exponential factor, E_a is the activation energy, and D is the mass diffusion coefficient. We assume that kinematic viscosity, diffusion, and heat conduction coefficients are dependent on temperature. Also, non-dimensional Lewis, Prandtl, and Schmidt numbers are assumed to be unity, as these assumptions do not affect the physical changes in the flame structures, partial flame extinguishing, and outbreak of distributed flames [4]. For description of an incident shock wave, we use uniform shocked flow condition with parameters (P_s, ρ_s, and T_s) determined from the Rankine-Hugoniot conditions for a given Mach number as shown in equation (7).

$$\begin{aligned}P_s&=P_0\left(\frac{2\gamma M_s^2}{\gamma+1}-\frac{\gamma-1}{\gamma+1}\right)\quad \rho_s=\rho_0\left(\frac{\left(\frac{\gamma+1}{\gamma-1}\right)\frac{P_2}{P_1}+1}{\left(\frac{\gamma+1}{\gamma-1}\right)+\frac{P_2}{P_1}}\right)\quad T_s\\&=T_0\left(\frac{\left(1+\frac{\gamma-1}{2}M_s^2\right)\left(\frac{2\gamma}{\gamma-1}M_s^2-1\right)}{\frac{(\gamma+1)^2}{2(\gamma-1)}M_s^2}\right)\end{aligned} \tag{7}$$

Convection is handled by the convex Essentially Non-Oscillatory (CENO) method rather than the weighted ENO (WENO) method due to its efficiency and robustness in simulating strong shock dominant phenomena for spatial discretization, and a third-order Runge-Kutta (RK) integration is used for temporal discretization [10]. Viscous, heat conduction, and mass diffusion fluxes are evaluated using the second-order finite difference method. The subgrid models are not considered for small turbulent eddies. Instead, the

numerical viscosity (especially RM instability) for the turbulent-energy dissipation is utilized as the effect of RM instability becomes roughly twice as large as the Kolmogorov decay in contribution to the characteristic scale of eddy vortices [4]. For efficient computing time, structured adaptive mesh refinement (SAMR) would help the present 2D simulation with single step chemistry achieve a 3D extension with detailed chemistry when needed in the future [11]. Regardless, present results are obtained without such use of SAMR.

2.2. *Problem setup*

We considered the stoichiometric ethylene-air mixture for flame acceleration and DDT initiation by the interaction between flame and shock in tubes. The initial temperature, pressure, density, mass fraction of reactant, and molecular weight are 293 K, 0.0133 MPa, 0.158 kg/m^3, 1, and 29 $\times$ 10^{-3} kg/mol, respectively. A single step reaction, $\dot{w}_i = A\rho Y \exp(-E_a/(RT))$ is chosen based on its feasibility to accurately resolve key length and time scales involved in the deflagration to detonation transition. Using theoretical equations based on adiabatic flame temperature 2625 K and CJ detonation velocity 1870 m/s, we determine heat capacity ratio as 1.15 and chemical energy release to be 48.824RT$_0$/M. Also, pre-exponential factor is set 3.2 $\times$ 10^8 m^3/kg$\cdot$s, and activation energy is 35.351RT$_0$ by solving the energy equation in laminar flame condition (laminar flame velocity: 1.28 m/s, and thickness: 0.96 mm) and by using a 1D detonation model (half-reaction thickness, 1.46 mm based on ZND theory and the given initial conditions) [4].

For handling the complex multi-material boundary conditions, we use level-set-based high-order ghost fluid method (GFM) for separating the gaseous mixture from the rigid tube wall. For natural handling of interfaces, ghost nodes of a combustible gas extended to the tube wall have the same entropies as the gas mixture [10]. The variables in the ghost nodes are extrapolated from the interior (gas side), while the velocity is set to the real node values and zero in the rigid wall for considering a boundary layer effect. Through a GFM process, we determine the velocity, density, species ratio, and internal energy of the ghost nodes. Pressure is determined

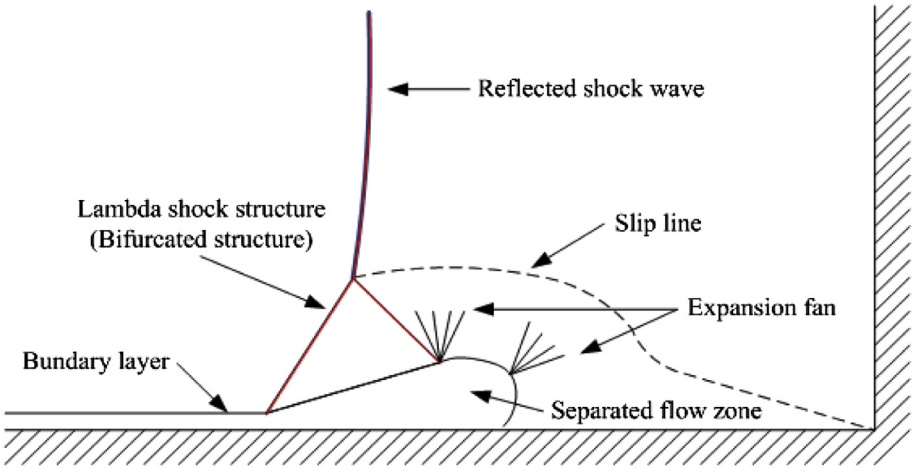

(a) Schematic diagram of lambda shock structure (bifurcated foot) [12]

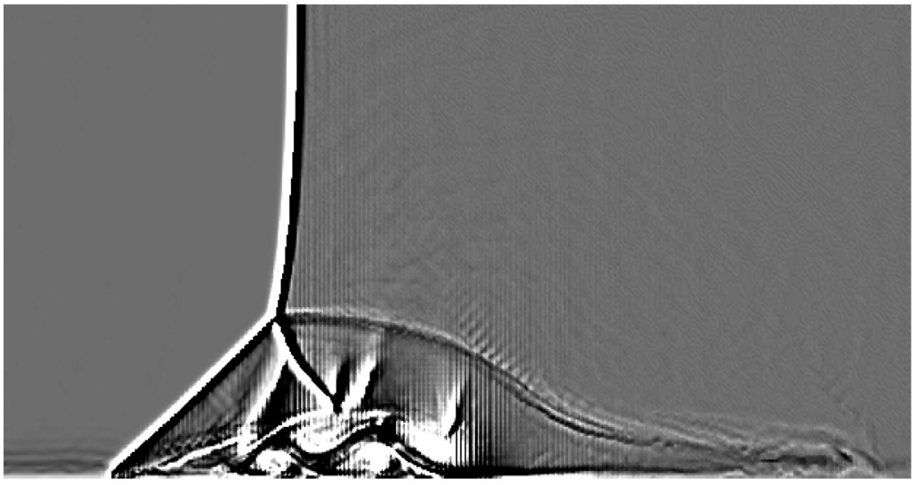

(b) Calculation

Fig. 1 – Schematic diagram and numerical shadowgraph of lambda shock structure induced by reflected shock and boundary layer interaction (a) Schematic diagram of lambda shock structure (bifurcated foot) [12] (b) Calculation.

from the equation of state. To identify the boundary layer effect in the near wall, we compute the formation of lambda shock structure (bifurcated foot) that results from interaction between reflected shock and boundary layer. Fig. 1 shows the schematic diagram and numerical shadowgraph of the lambda shock structure. The numerical shadowgraph describes the key features of a lambda shock consisting of slip line, expansion wave, and recirculation zone [12].

The complex confinement effects at the onset of DDT are investigated through various combinations of wall turning in the flow downstream, varying size of obstacle within tube, and initial flame size. So we make comparison of four different geometrical confinements by their types: Type-(I) Straight tube with no obstacle Type-(II) Straight tube with obstacles Type-(III) Bent tube with no obstacle Type-(IV) Bent tube with obstacles.

We configured the bends with obstacles to confirm the effects of curved wall and obstacle size. The numerical domain of the bent tube is 90 mm by 145 mm, with entire tube length being 242 mm based on the centerline length of an 'equivalent' straight tube (see Fig. 2). The incident shock is initially placed 8 mm from the left inlet. A uniform flow is assumed in the post-shock state between the left boundary and the incident shock. The center of a circular flame is initially located at 20 mm from the left, and its initial diameter is 20 mm. The initial flame is assumed to have a discontinuity, where the adiabatic flame conditions (temperature, 2625 K and density, 0.0177 kg/m^3) are separated from the surrounding ambient conditions. In a bent region, the outer and inner radiuses are 40 mm and 10 mm, respectively. We considered 3 different obstacle sizes (height of $h = 0$ (smooth), 2.5 (small obstacle), and 5 mm (large obstacle)), and tested three different initial flame sizes (radiuses of 9, 10, and 11 mm) in the tube. In our model, zero gradient inflow/outflow boundary conditions are applied at inlet and exit in order to prevent any interference with rarefaction or shock reflection on the

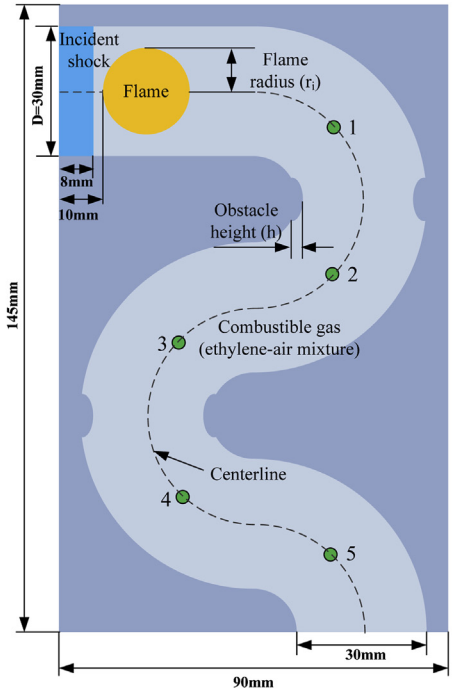

(a) Bent tube – Type-(III, IV)

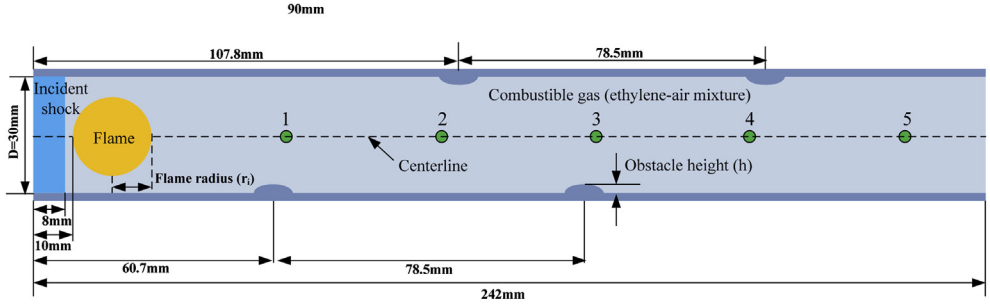

(b) Straight tube – Type–(I, II)

Fig. 2 – Schematic of (a) bent tube and (b) straight tube, both with varying obstacle size ($h = 0$ (smooth), 2.5 (small), and 5 mm (large)). Pressure gauges are located at 1 (64.2 mm), 2 (103.6 mm), 3 (143 mm), 4 (182 mm), and 5 (221.4 mm) from left inlet along centerline.

shock–flame interaction. For comparison of the pressure variation with a straight tube, we use five pressure gauges placed at equidistance from each other along the center axis as shown in Fig. 2.

3. Results and discussion

We performed DDT simulation of a stoichiometric ethylene-air mixture subject to a variety of incident shock intensities at Mach numbers ranging from 1.9 to 2.7. The effect of wall obstacles is considered with three different obstacle sizes, and the different initial flame size is also tested.

3.1. *Validation and grid resolution test*

Ref [13]. showed shock-induced ethylene-air experiment in a straight tube without the obstacle. Fig. 3 is a pressure history from the experiment as compared to our calculation. Calculated pressure represents peak pressures sampled in the center of tube where as the experiment is pressure taken near the wall. Comparison is in good agreement in terms of maximum pressure near 1.2 MPa, overall decreasing tendency, and tail pressure being ~0.4 MPa. Noticeable fluctuations are observed in both cases where complex wall reflections of shocks are presumed responsible. Additionally, our calculation suggests that velocity and pressure of the strange wave are approximately 932 m/s and 0.52 MPa, respectively. Table 1 shows a comparison of the velocity and pressure of strange wave versus detonation from the reference, suggesting a strong agreement between experiment and calculation.

The reaction zone thickness is carefully resolved by requiring a mesh size to be 0.1 mm. Three levels of grid refinements (0.2, 0.1, and 0.05 mm) were tested for checking grid independence, and 0.1 mm was chosen to be optimal for hot spot identification in the flame zone. This resolution corresponds to approximately 10 computational cells in the ethylene-air mixture's laminar flame thickness of about 0.96 mm [4]. Fig. 4 shows a history of the energy release rate (J/(mm^3 K)) in accordance with three mesh resolutions for the case of $Ma = 2.7$ bent tube with large obstacle. The detonation transition time and position for both resolutions 0.1 mm and 0.05 mm are 0.101 ms and at the corner of first obstacle, respectively.

Table 1 – Comparison of reference and numerical values of strange wave and detonation in ethylene-air mixture under intensity of incident shock, $Ma = 2.5$

		Reference [4,13]	Numerical
Strange wave	Pressure, MPa	0.53	0.52
	Velocity, m/s	~850	932
Detonation	Pressure, MPa	1.2	1.33
	Velocity, m/s	CJ, 1870	2076

3.2. *Effect of curved wall in tube bends*

The effect of curved wall on DDT is considered by making comparison of a multi bend to a straight tube. In general, the multi-interaction between boundary layer, shock, and flame gives rise to hot spot formation, which can trigger an auto-ignition and a detonation transition. In a straight tube long enough to clear the minimum distance needed for a DDT for an ethylene-air mixture, the detonation transition will always occur in the case of a strong shock intensity (roughly $Ma > 2.5$). However, we used a shorter test tube (242 mm) in which no transition can occur regardless of the incident shock strength, while we observed DDT in a bent tube subject to a weak shock intensity at $Ma = 2.1$.

The temperature and pressure fields in a smooth bent tube subject to $Ma = 2.1$ are shown in Fig. 5. The flame is distorted and expanded by a shock and flame interaction due to presence of the curved walls (see Fig. 5(a)). During this process, the

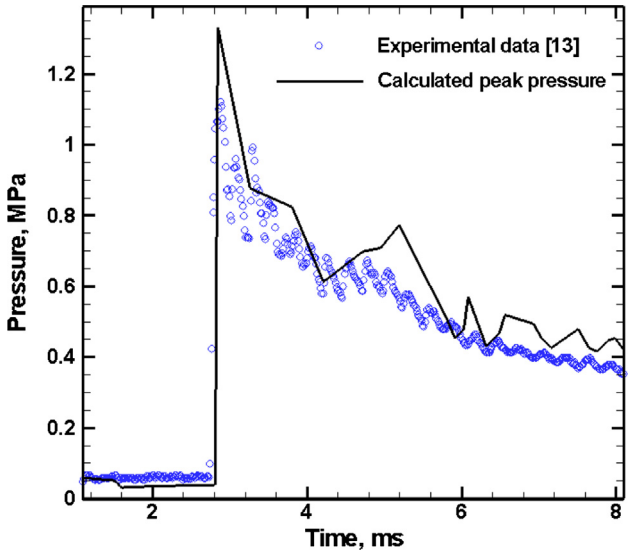

Fig. 3 – Verification of pressure history from experiment and calculation.

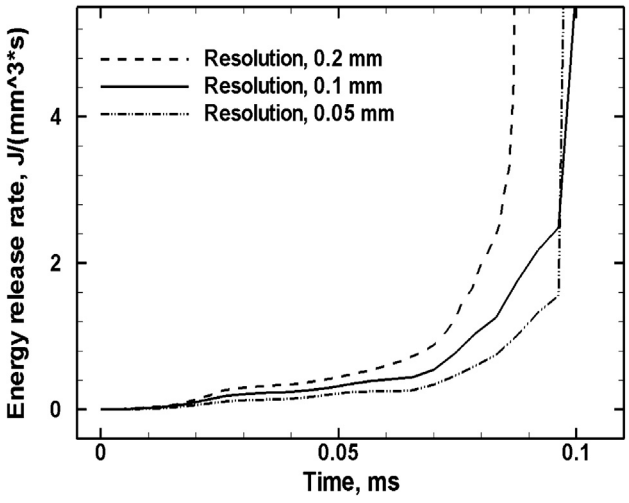

Fig. 4 – Comparison between detonation transition times from 0.2, 0.1, and 0.05 mm resolutions for $Ma = 2.7$.

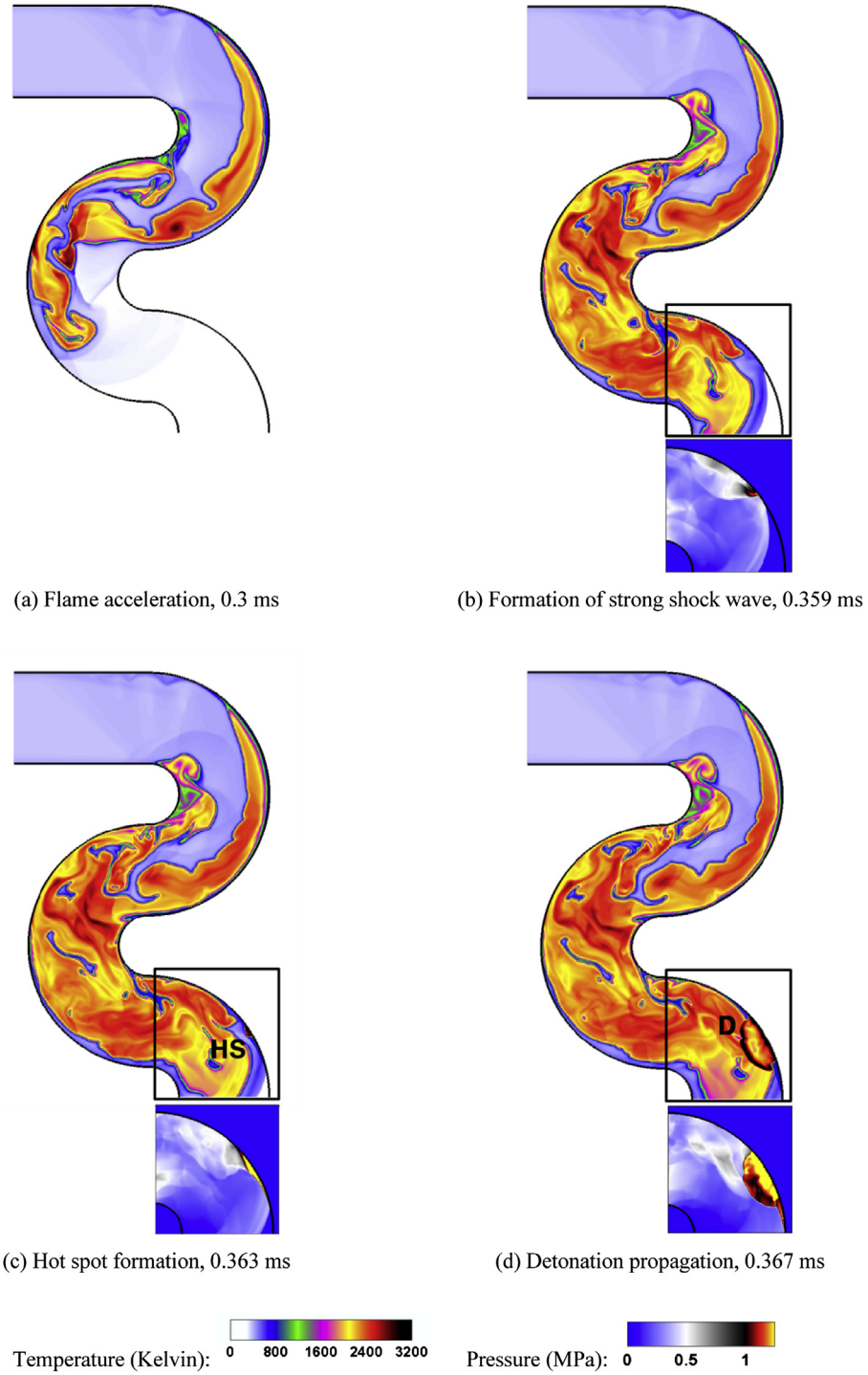

Fig. 5 – Temperature and pressure (in separate window) under $Ma = 2.1$ incident shock interacting with an ethylene-air flame in Type-(III) tube. HS and D mean hot spot and detonation, respectively (a) Flame acceleration, 0.3 ms (b) Formation of strong shock wave, 0.359 ms (c) Hot spot formation, 0.363 ms (d) Detonation propagation, 0.367 ms.

shock is strengthened forming a strange wave packet. This enhanced shock strength generates hot spots near the surface of the curved wall. In both Fig. 5(b) and (c), the strange wave propagates downstream, and it is noticeably reinforced; the wave intensity is strengthened while propagating along the curved wall. Eventually, a hot spot is generated at a specific location on the wall at 0.363 ms. Hence, detonation propagates outwards toward the surrounding from this point onwards (see Fig. 5(d)).

Next, we consider a strong shock intensity at $Ma = 2.7$, as shown in temperature and pressure fields of Fig. 6. The first detonation transition appears near the second curved wall

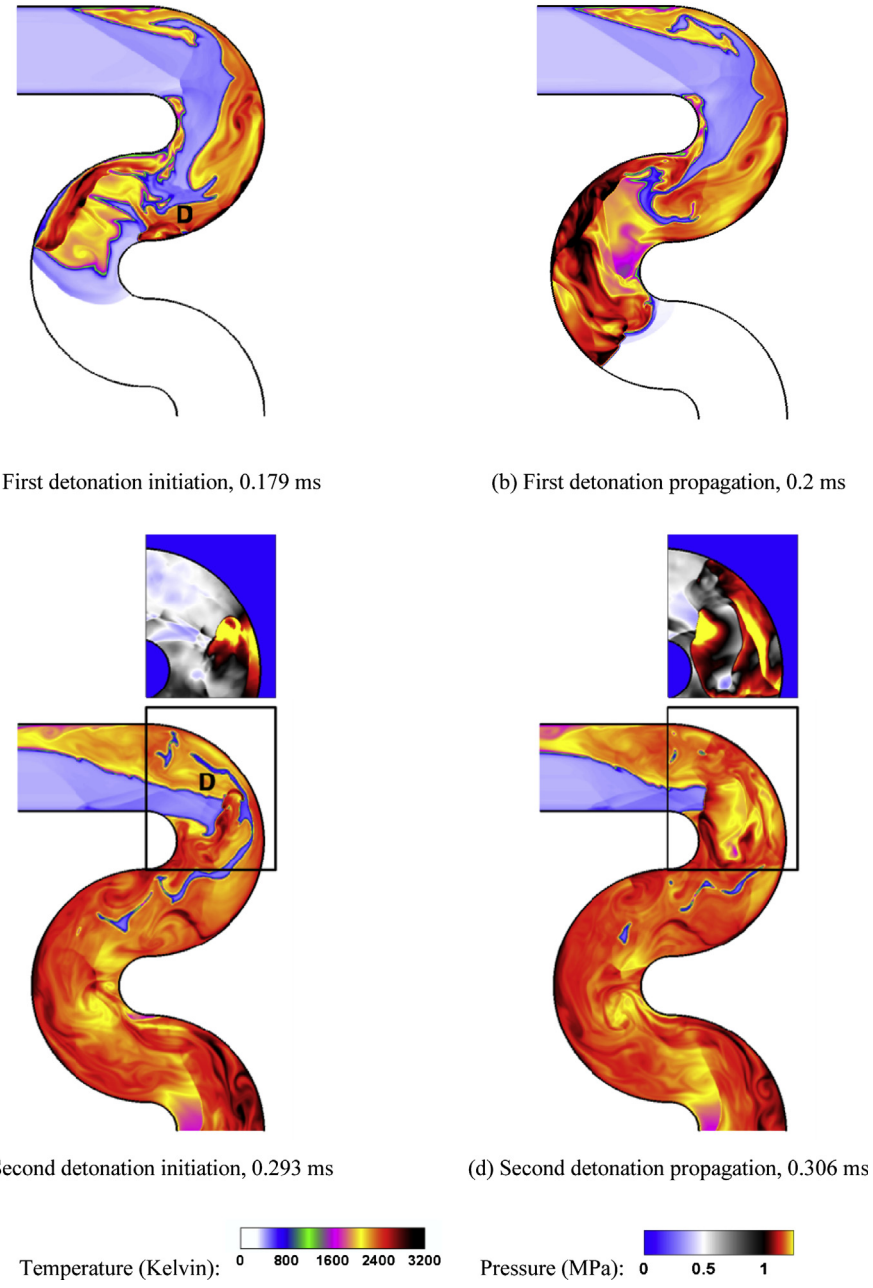

Fig. 6 – Temperature and pressure (in separate window) under $Ma = 2.7$ incident shock interacting with an ethylene-air flame in Type-(III) tube (a) First detonation initiation, 0.179 ms (b) First detonation propagation, 0.2 ms (c) Second detonation initiation, 0.293 ms (d) Second detonation propagation, 0.306 ms.

at 0.179 ms and leading shock wave is attached to a reaction front (see Fig. 6(a) and (b)). However, this flame does not propagate upstream because of opposite walls and the absence of reactants. In Fig. 6(c) and (d), a retonation wave propagates upstream along the wall near the flame. Then, the wave makes contact with two flame tips and repeatedly interacts with flames and the curved wall. Through this process, a hot spot is formed between two flame tips, and a second detonation is triggered from this point. In order to confirm the curved wall effect, we compare this observation to a straight tube under the same shock intensity at $Ma = 2.7$.

Fig. 7 shows pressure histories of all 4 tubes as tested at 5 gauge locations. For starter, we look at tubes with no obstacles which correspond to lines (I) and (III). By inspection, bent tube-(III) pressure fluctuates and is significantly increased due to the propagation of a strong shock wave and detonation. The peak pressure also does not exceed CJ detonation pressure for (III) since reactants burn out before detonation occurs. However, the emerging strange wave is

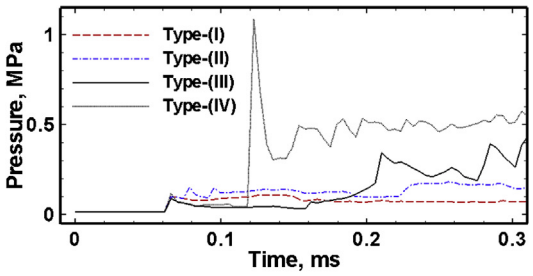

(a) Gauge 1 (64.2 mm)

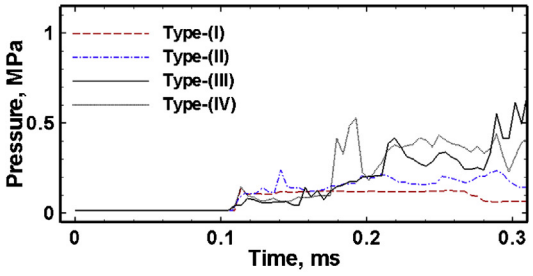

(b) Gauge 2 (103.6 mm)

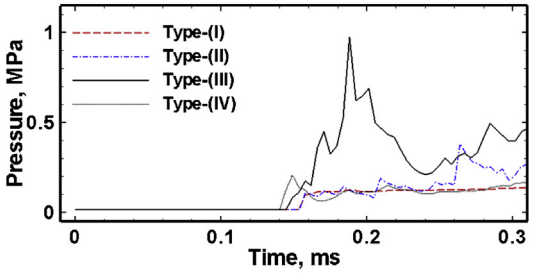

(c) Gauge 3 (143 mm)

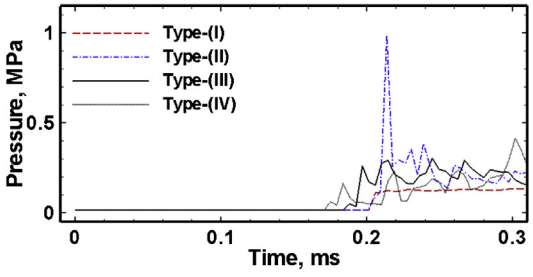

(d) Gauge 4 (182 mm)

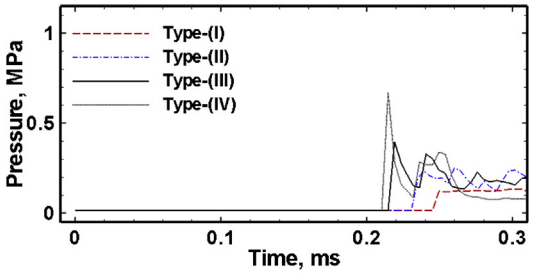

(e) Gauge 5 (221.4 mm)

Fig. 7 – Pressure histories shown by tube types taken at every 500 cycles for *Ma* = 2.7 case: Type-(I) Straight no obstacle; Type-(II) Straight with obstacle; Type-(III) Bend no obstacle; Type-(IV) Bend with obstacle. (a) Gauge 1 (64.2 mm) (b) Gauge 2 (103.6 mm) (c) Gauge 3 (143 mm) (d) Gauge 4 (182 mm) (e) Gauge 5 (221.4 mm).

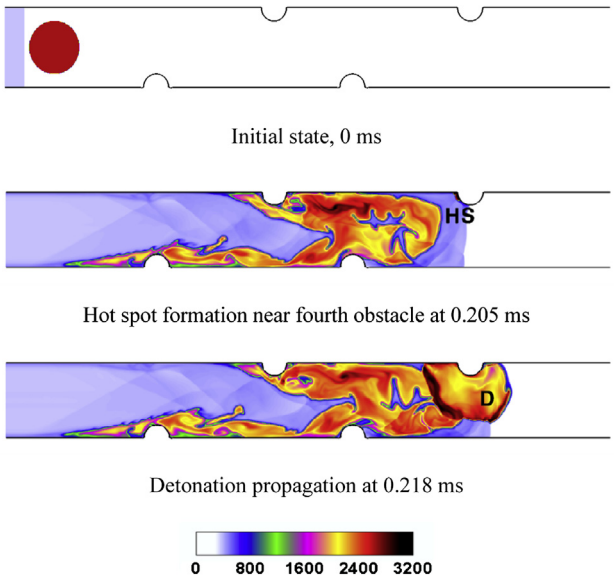

Fig. 8 – Straight tube with four obstacles (*h* = 5 mm) showing temperature (Kelvin) field. *Ma* = 2.7 incident shock accelerated flame of ethylene-air mixture developing into a detonation at time 0.218 ms.

confirmed as the pressure ranges from 0.4 to 1.1 MPa at time 0.293 ms. At locations different from gauging points, detonation pressures ranging from 0.6 to 2.7 MPa (CJ detonation pressure being 1.2 MPa) are shown for bent tube-(III) in Fig. 6(c)–(d). The pressure fluctuation is due to shock disturbances and release of the chemical energy of reactant. The pressure increases beyond 2 MPa in the reactant-rich flow condition, whereas the magnitude of pressure increase is below 1 MPa in the reactant-deficient condition. Pressure signals for straight tube-(I) remains smooth throughout, showing no sign of DDT.

3.3. *Effect of obstacle size in bent tube*

The straight tube with obstacles is a 242 mm by 30 mm in dimension with no-slip wall condition, using four obstacles positioned at 60.7, 107.8, 139.2 and 186.5 mm. Obstacles of the bent tube are also positioned at the same 4 locations along the wall curvature of a total running length of 242 mm (see Fig. 2(b)). Fig. 8 shows temperature field of Type-(II), a straight tube with large obstacle (*h* = 5 mm), using an incident shock wave, *Ma* = 2.7. In the figure, at 0.205 ms, a detonation occurs in front of a fourth obstacle. This suggests that detonation transition time and distance of straight tube with obstacle are 0.205 ms and 181.11 mm, which are much shorter than the straight tube case. However, these are longer than Type-(IV), bent tube with obstacles (0.1 ms, 81.65 mm) and Type-(III) without obstacles

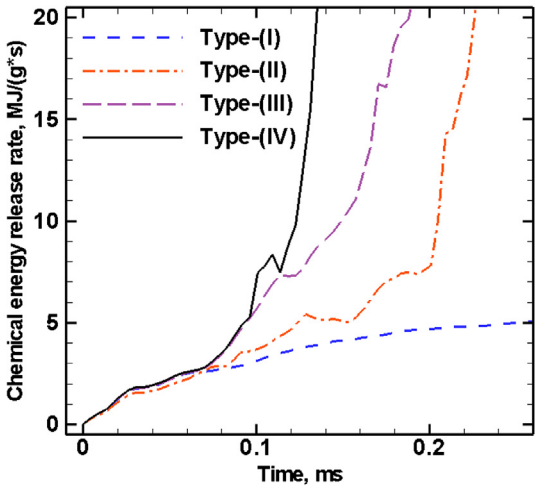

Fig. 9 – Comparison of energy release rate for different tube types under *Ma* = 2.7 incident shock.

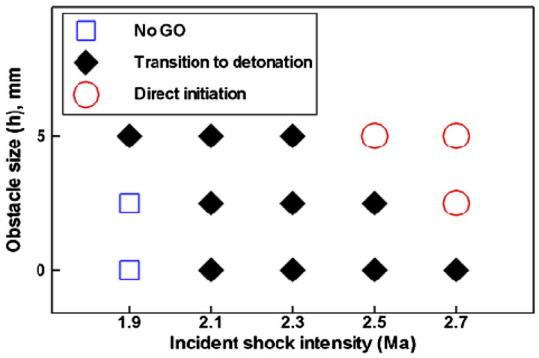

Fig. 11 – GO/No GO map on incident shock strength and obstacle size of the bent tube.

(0.162 ms, 119.32 mm) based on a jump in the chemical energy release rate (see Fig. 9). Therefore the curved wall is an effective means of a detonation transition, and thus the combination of curved wall with obstacles or Type-(IV) is an optimal choice.

Fig. 7 depicts pressure histories of all 4 type tubes as tested at five gauges (64.2, 103.6, 143, 182, and 221.4 mm from inlet). From the pressure records, detonation transition distance and time can be inferred. Type-(IV), bent tube with obstacles, develops detonation in a shortest distance and time (see Fig. 7(a)).

Fig. 10 shows the transition distance of Type-(III) and (IV) with different obstacle sizes (h = 0, 2.5, and 5 mm) and varying incident shock strength. The detonation distance is decreased along the increasing obstacle size and incident shock intensity. This tendency shown in Fig. 11 also presents a GO/No GO region on the plane of incident shock strength versus obstacle size. The obstacle effect in Type-(IV) is checked through a comparison with the chemical heat release rates of smooth Type-(III). Fig. 12 shows that the detonation transition in the large obstacle case (at 0.324 ms) is faster than the smooth case (at 0.363 ms) as seen in the first peak appearing time. In the large obstacle case, the peak value near 20 MJ/(g·s) is reached from 0.29 to 0.36 ms and at 0.486 ms, corresponding to a first and second detonation. Here, the chemical energy release rate is approximately 20 MJ/g·s when detonation transition occurs, which is the same for both smooth and small obstacle cases. In the smooth case, the peak is shown at 0.363 ms upon detonation, after which the chemical heat release rate is sustained at almost half of the peak value near 10 MJ/(g·s).

Fig. 13 shows flame propagation details of small and large obstacle cases at *Ma* = 2.5. In comparison, the formation of hot spots and direct initiation from these hot spots in each case are observed. In the small obstacle case, a hot spot did not directly initiate a detonation (see Fig. 13(a), (b)), due to insufficient reactants at a pressure of 0.9 MPa and at

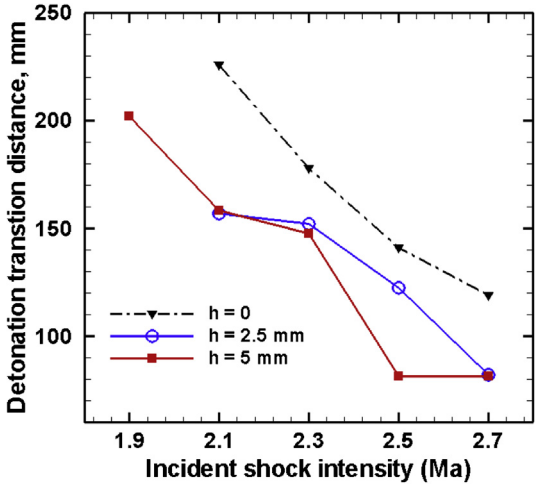

Fig. 10 – Comparison of detonation transition distance in Type-(III, IV) with obstacle size (h = 0, 2.5, and 5 mm) and varying incident shock strength.

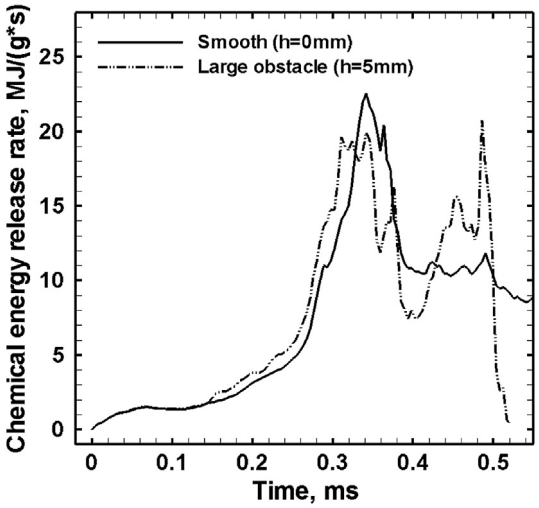

Fig. 12 – Comparison of chemical energy release rate in Type-(III, IV) under *Ma* = 2.1.

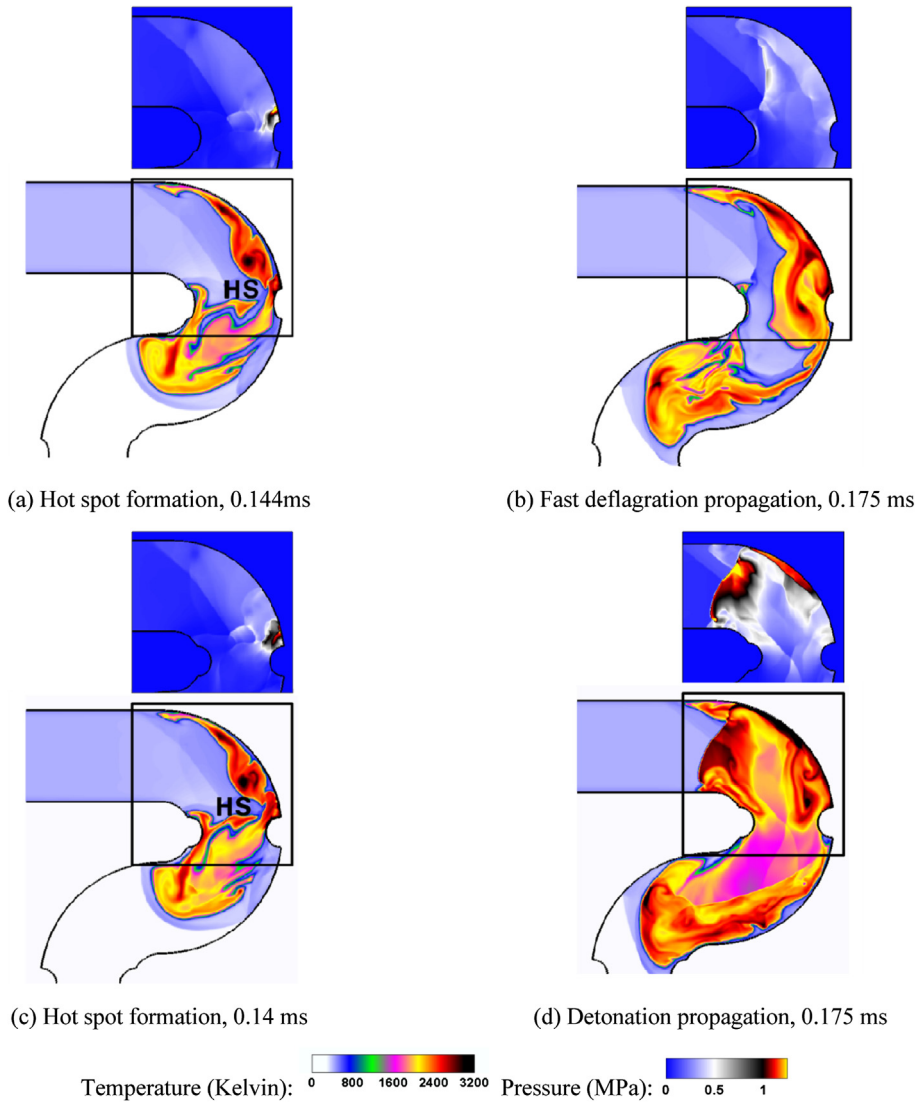

Fig. 13 – Obstacle size comparison. Temperature and pressure (in separate window) under $Ma = 2.5$ incident shock interacting with an ethylene-air flame in Type-(IV) with obstacles ($h = 2.5$ mm: (a)–(b), $h = 5$ mm: (c)–(d)). (a) Hot spot formation, 0.144 ms (b) Fast deflagration propagation, 0.175 ms (c) Hot spot formation, 0.14 ms (d) Detonation propagation, 0.175 ms.

temperature of 600 K. In the large obstacle case, however, hot spot can initiate a direct detonation (see Fig. 13(c),(d)) because of a sufficiently high pressure of 1 MPa and temperature of 900 K. Hot spots of both cases are observed at nearly identical locations with similar intensity. Nevertheless, direct initiation differed due to the flame shape, intensity of the shock reflection, and shock–flame interactions, which are influenced by the differences in confinement geometry.

3.4. *Effect of initial flame size in bent tube with obstacles*

To confirm the effect of initial flame size, we consider three different flame radii ($r_f = 9$, 10, and 11 mm). Fig. 14 shows the first detonation transition time and distance for each case. The time to detonation is decreased regardless of flame size for increasing shock intensity. The initial flame size either accelerates or delays the transition to a detonation under different incident shock intensities. In the weak incident shock condition (below Mach 2.3), the detonation transition in large flame is slightly faster because of the initially wider flame surface that induces acceleration of the shock and the flame. The small flame results in delayed transition because of low temperature (750 K), pressure (0.82 MPa), and reactant fraction at $Ma = 2.3$. The detonation transition in a small incident flame does not occur at $Ma = 2.1$. However, in the strong incident shock condition ($Ma = 2.5$), the larger initial flame leads to a delayed transition due to the absence of reactants in the regions of complex confinement, such that the detonation transition in large flame is slow. In Fig. 15(a) and (b), pressure field shows detonation transition at 0.241 ms, which is different from Fig. 15(c). This noticeable effect of

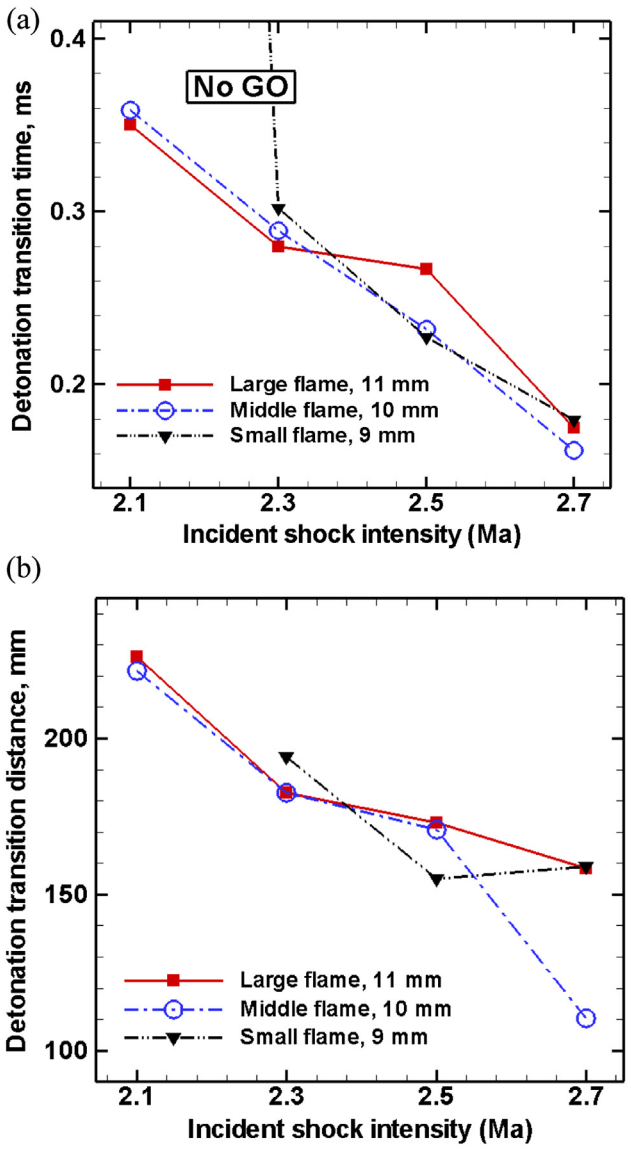

Fig. 14 – Comparison of detonation transition (a) time and (b) distance in Type-(III) for different initial flame size and varying incident shock strength tested.

initial flame size is shown to depend closely on the surrounding geometry.

4. Conclusion

We confirm that the shock–flame interaction by the effects of complex confinement geometry (curved wall and obstacle) and initial flame size is critical for detonation transition of the shock-accelerated ethylene-air flame. The simulations of straight tubes and bent tubes with obstacles show generation of the hot spots on walls or flame tips through multiple shock–flame interactions. Our simulations indicate that the multi bends have advantage over the straight tube with obstacles in the detonation transition, and the initial flame size also plays a deciding role. Thus, flame propagation and DDT may be restrained or accelerated by the multi bend effects with obstacles and the initial flame size. Furthermore, when the chemical heat release rate averaged from the entire tube reaches above 20 MJ/(g·s), the first detonation transition is always observed. Such transition time is delayed due to the absence of reactant and insufficient pressure and temperature required for initiation. This suggests that instantaneous flame spread interrupts the initiation of detonation even though the hot spots are already formed. Our DDT study of hydrocarbon mixture on both geometrical conditions and initial flame size has strong potential for enhancing the performance of a pulsed detonation engine and providing countermeasures that allow operators of nuclear power plants to avoid fatal flame accelerations or DDT. Furthermore, different fuel mixtures, deformable wall conditions, and realistic geometries in three dimensions are required for further understanding of such a complex transition process of hydrocarbon mixture in combustion.

Acknowledgments

The authors are thankful for the financial support from the Hyundai Motor Group and ADD through the Institute of Advanced Aerospace Technology at Seoul National University.

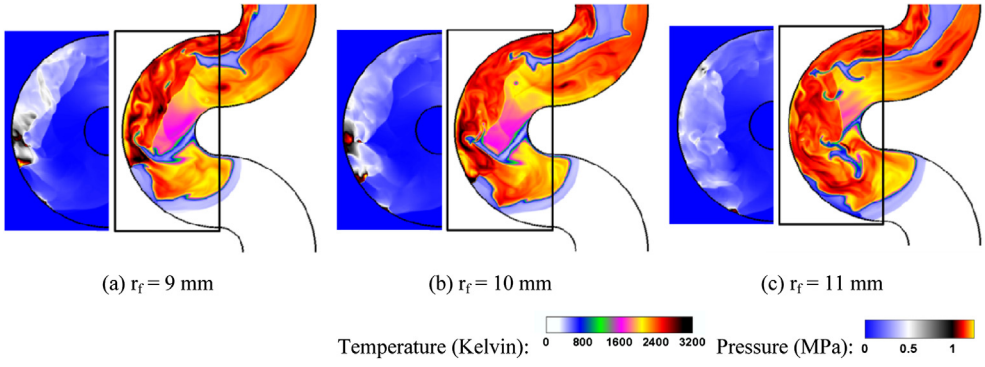

Fig. 15 – Initial flame size comparison. Temperature and pressure (in separate window) under $Ma = 2.5$ incident shock interacting with an ethylene-air flame in Type-(III) for different initial flame size r_f ((a), (b): detonation; (c): fast deflagration at 0.241 ms).

REFERENCES

[1] Kim DH, Yoh JJ. Predictive model of onset of pipe failure due to a detonation of hydrogen-air and hydrocarbon-air mixtures. Int J Hydrogen Energy 2009;34:1613–9.

[2] Vaidogas ER, Juocevicius V. Sustainable development and major industrial accidents: the beneficial role of risk-oriented structural engineering. Technol Econ Dev Econ 2008;14(4):612–27.

[3] Dzieminska E, Hayashi AK. Auto-ignition and DDT driven by shock wave – boundary layer interaction in oxyhydrogen mixture. Int J Hydrogen Enegy 2013;38:4185–93.

[4] Oran ES, Gamezo VN. Origins of the deflagration-to-detonation transition in gas-phase combustion. Combust Flame 2007;148:4–47.

[5] Ciccarelli G, Dorofeev S. Flame acceleration and transition to detonation in ducts. Prog Energy Combust Sci 2008;34:499–550.

[6] Liberman MA, Ivanov MF, Kiverin AD, Kuznetsov MS, Chukalovsky AA, Rakhimova TV. Deflagration-to-detonation transition in highly reactive combustible mixtures. Acta Astronaut 2010;67:688–701.

[7] Zel'dovich YAB. Regime classification of exothermic reaction with nonuniform initial condition. Combust Flame 1980;39:211–4.

[8] Frolov SM, Aksenov VS, Shamshin IO. Shock wave and detonation propagation through U-bend tubes. Proc Combust Inst 2007;31:2421–8.

[9] Otsuka S, Suzuki M, Yamamoto M. Numerical investigation on detonation wave through U-bend. J Therm Sci 2010;19:540–4.

[10] Kim K, Yoh JJ. A particle level-set based Eulerian method for multi-material detonation simulation of high explosive and metal confinements. Proc Combust Inst 2013;34(2):2025–33.

[11] Ziegler JL, Deiterding R, Spheherd JE, Pullin DI. An adaptive high-order hybrid scheme for compressive, viscous flows with detailed chemistry. J Comput Phys 2011;230:7598–630.

[12] Davies L, Wilson JL. Influence of reflected shock and boundarylayer interaction on shock tube flows. Phys Fluids 1969;12:1–37.

[13] Thomas G, Bambrey R, Brown C. Experimental observations of flame acceleration and transition to detonation following shock-flame interaction. Combust Theor Model 2011;5:573–94.